NUCL SCI TECH (2019) 30:83
https://doi.org/10.1007/s41365-019-0597-z

^{18}F-PBR06 PET/CT imaging of inflammation and differentiation of lung cancer in mice

He Zhang[1,2,3] · Hui Tan[1,2,3] · Wu-Jian Mao[1,2,3] · Jun Zhou[1,2,3] · Zhe-Quan Fu[1,2,3] · Yan Hu[1,2,3] · Jie Xiao[1,2,3] · Qing-Yu Lin[1,2,3] · Hong-Cheng Shi[1,2,3] · Deng-Feng Cheng[1,2,3]

Received: 21 October 2018 / Revised: 8 November 2018 / Accepted: 9 November 2018 / Published online: 20 April 2019

Abstract The present study explored the 18-kDa translocator protein radioligand ^{18}F-PBR06 as a PET imaging biomarker for diagnosis of inflammation and compared it with ^{18}F-FDG for differentiation of inflammation and lung tumors in animals. ^{18}F-PBR06 was synthesized with an average decay-corrected radiochemical yield of 30–40% (end of synthesis, EOS), and the radiochemical purity was greater than 99%. The inflammation-to-blood ratio of ^{18}F-PBR06 (3.53 ± 0.26) was higher than the tumor-to-blood ratio (1.77 ± 0.35) ($P < 0.001$). The inflammation-to-muscle ratio of ^{18}F-PBR06 (2.33 ± 0.64) was also higher than the tumor-to-muscle ratio (1.45 ± 0.14) ($P = 0.036$). Micro-PET/CT images showed high uptake of ^{18}F-FDG in both inflamed muscles and lung tumor tissues. However, ^{18}F-PBR06 uptake in inflamed muscles remained higher than that in the lung tumor tissues, following 90 min of dynamic Micro-PET/CT imaging. Further, macrophages in the inflammatory regions showed a higher fluorescence signal than in lung tumor tissues. Results of the study confirmed that ^{18}F-PBR06 PET/CT imaging allowed for diagnosis of inflammation. Moreover, ^{18}F-PBR06 uptake in the inflammatory regions was significantly higher than in lung tumor tissues, suggesting that ^{18}F-PBR06 PET/CT imaging has potential to differentiate between peripheral lung cancer and inflammation nodules.

Keywords TSPO · Macrophage · PET/CT · Inflammation · Lung cancer

1 Introduction

Inflammation is a common defense reaction to injury in vascularized living tissues, which is shared by many diseases [1]. Positron emission tomography (PET) imaging using fluorine-18-fluorodeoxyglucose (^{18}F-FDG) has been widely used to evaluate focal and generalized infectious and inflammatory disorders [2]. Further, ^{18}F-FDG PET/CT imaging has been widely used in tumor detection, staging, and therapy response monitoring [3, 4]. Therefore, inflammation-specific imaging tracers are needed to provide more accurate diagnosis of inflammatory diseases and better understanding of the pathological process.

Accurate pulmonary nodule detection is a crucial step in diagnosing pulmonary cancer [5]. Currently, differentiating peripheral lung cancer and inflammation nodules remains a fundamental unsolved problem [6]. Alternative methods for distinguishing between peripheral lung cancer and inflammation nodules include delayed PET/CT imaging of ^{18}F-FDG uptake [7]. However, results of delayed ^{18}F-FDG PET/CT imaging may provide additional false positive

This work was funded in part by the National Natural Science Foundation of China (Nos. 11875114, 81471706, and 81871407), Science and Technology Commission of Shanghai Municipality (No. 16410722700), and sponsored by the Shanghai Sailing Program (No. 17YF1417400).

✉ Hong-Cheng Shi
shihongcheng163@163.com

✉ Deng-Feng Cheng
cheng.dengfeng@zs-hospital.sh.cn

[1] Shanghai Institute of Medical Imaging, Shanghai 200032, China

[2] Department of Nuclear Medicine, Zhongshan Hospital, Fudan University, Shanghai 200032, China

[3] Institute of Nuclear Medicine, Fudan University, Shanghai 200032, China

results due to its low specificity. Thus, it is essential to develop an inflammation-specific tracer to provide more accurate diagnosis of pulmonary cancer.

Furthermore, macrophages play a significant role in inflammation progression [8]. In inflammation progression, macrophages are activated to defend against invasive pathogens. Following activation, the recruited macrophages act either as defenders against invasive pathogens or promoters to stimulate local inflammatory responses by releasing various chemokines and cytokines, thereby serving as appropriate biological targets for inflammation-specific PET imaging tracers [9, 10].

The translocator protein (TSPO), also known as peripheral benzodiazepine receptor (PBR), is a 18-kDa outer mitochondrial membrane protein that participates in the regulation of numerous cellular processes, including cholesterol metabolism, steroid biosynthesis, cellular proliferation, and apoptosis [11, 12]. This protein is localized on the outer mitochondrial membrane of several cell types, including macrophages, neutrophils, and glioma cells, and has been shown to exhibit low expression in many tumor cells [11, 12]. This evidence indicated that TSPO tracers have greater potential as tracers to specifically target inflammation and to differentiate between peripheral lung cancer and inflammation nodules. ^{18}F-*N*-fluoroacetyl-*N*-(2,5-dimethoxybenzyl)-2-phenoxyaniline (^{18}F-PBR06) is a second-generation PET-targeting TSPO tracer, which has been used in human studies, and has increased binding affinity, higher signal-to-noise ratio, and low lipophilicity [12–14]. Previously, ^{18}F-PBR06 has displayed high uptake in neuroinflammation [15]; however, the potential to detect inflammation in peripheral tissues has not yet been evaluated.

In this study, we performed Micro-PET/CT imaging using ^{18}F-PBR06 and ^{18}F-FDG in rodent lung tumor and inflammation models. Herein, we aimed to investigate the feasibility of these tracers to detect and differentiate between inflammation and lung tumors.

2 Materials and methods

2.1 Synthesis of PET tracers

The radiotracer ^{18}F-FDG was manufactured via a fully automated FDG MX module (GE Medical Systems, Germany). The radiochemical purity of ^{18}F-FDG was $> 98\%$.

An automated TRACERlab $FX_{F\text{-}N}$ radiosynthetic module (GE Medical Systems, USA) was used to prepare ^{18}F-PBR06 as previously reported [16]. Further, ^{18}F-PBR06 was synthesized using a novel tosylate precursor as described previously [17]. The synthetic procedures of ^{18}F-PBR06 are shown in Fig. 1a. Radiosynthesis of ^{18}F-PBR06 using the new tosylated precursor provided similar radiochemical purity, higher specific activity, and higher radiochemical yield in comparison with radiosynthesis using bromine precursor [17]. The decay-corrected radiochemical yields of ^{18}F-PBR06 were 30–40% (end of synthesis, EOS), and the radiochemical purity of ^{18}F-PBR06 was greater than 99%.

2.2 Animal models

The animal study protocol was in accordance with the principles and procedures outlined in the Guide for the Care and Use of Laboratory Animals and approved by Zhongshan Hospital. FVB/N (FVB) and athymic nude mice (both female, 6–8 weeks) were purchased from Peking University Laboratory Animal Center (Beijing, China). Each athymic nude moue was inoculated with 2×10^6 A549 lung cancer tumor cells to establish the lung cancer model. When the A549 tumor volumes in athymic nude mice reached 0.5 cm^3, the FVB mice were injected with 20 μL turpentine into the muscles of their left hind legs to establish the inflammation model. In total, 14 animals were used in the whole study. Three mice each of inflammation and lung cancer models were used for ^{18}F-FDG Micro-PET/CT imaging and ^{18}F-PBR06 Micro-PET/CT imaging. Subsequently, the animals were killed for immunofluorescence analysis (Fig. 1c). Further, additional four mice each of inflammation and lung cancer models were used for the biodistribution study. All mice were maintained in a temperature-controlled environment under a 12-h light/dark cycle with free access to food and water.

2.3 Biodistribution studies for ^{18}F-PBR06

The inflammation and lung cancer models were intravenously injected with 5.56 MBq of ^{18}F-PBR06 ($n = 4$) and killed 120 min later by ethyl ether anesthesia. Blood was collected from the heart, and normal tissues (kidneys, brain, liver, spleen, intestine, lung, stomach, pancreas, and muscles of the right hind leg), inflamed muscles, and A549 tumors were excised. All samples were weighed, and the radioactivity was measured by a GC-1200 gamma counter (HYMI-1403-015), followed by decay correction. Tracer accumulations of a three-dimensional region of interest (3D-ROI) for a volume were calculated as follows: 3D-ROI = (radioactivity of organs/radioactivity of injected drugs)/quality of organs. The results were expressed as the percentage of injected dose per gram of tissue (% ID/g).

2.4 Micro-PET/CT imaging

A Siemens Inveon Micro-PET/CT scanner (Siemens Preclinical Solutions, Knoxville, TN, USA) was used for

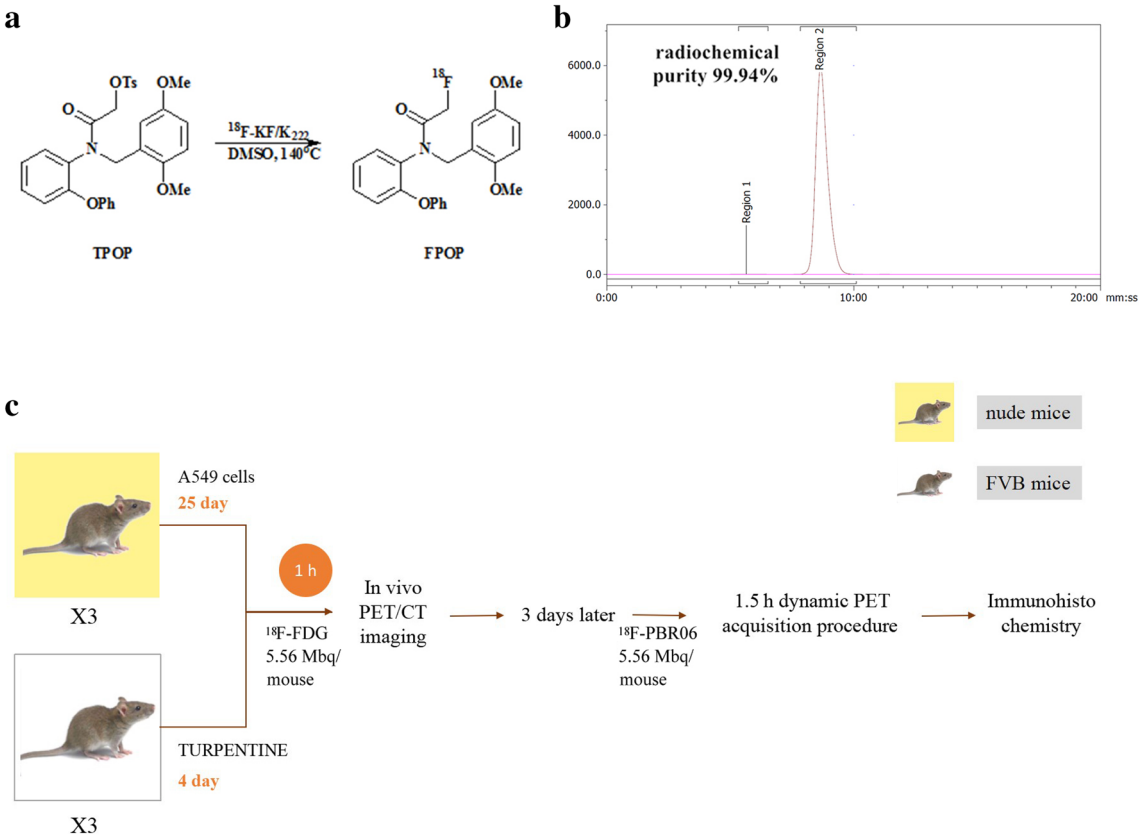

Fig. 1 **a** Synthetic procedures of ^{18}F-PBR06 using a novel tosylate precursor. **b** Radio-HPLC analysis of ^{18}F-PBR06. **c** Flow chart of the animal study design. Models of inflammation and lung cancer (n = 3 each) were used for ^{18}F-FDG Micro-PET/CT imaging, followed by ^{18}F-PBR06 Micro-PET/CT imaging 3 days later. Subsequently, the animals were killed for immunofluorescence analysis (Color online)

Micro-PET/CT scans and imaging analysis. For the inflammation models, 10-min PET images and 5-min CT images were acquired on day 4 post-injection of turpentine oil at 1 h following the 5.56 MBq ^{18}F-FDG injection via the tail vein. Furthermore, 1.5-h dynamic PET images and 5-min CT images were obtained on day 7 post-injection of turpentine oil following the 5.56 MBq ^{18}F-PBR06 injection via the tail vein. For the lung cancer models, 10-min PET images and 5-min CT images were performed at 1 h following the 5.56 MBq ^{18}F-FDG injection via the tail vein on day 25 post-inoculation. Subsequently, 1.5-h dynamic PET images and 5-min CT images were performed following the 5.56 MBq ^{18}F-PBR06 injection via the tail vein on day 28. The data were reconstructed using a 3D OSEM algorithm and segmented attenuation. 3D-ROIs were placed on the inflamed lesions or tumor tissues, and a threshold of 40% of the maximum uptake was used for the final ROI drawing.

2.5 Immunofluorescence

The inflammatory regions on day 7 after turpentine injection and lung cancer models on day 28 after inoculation into mice were excised and embedded in paraffin. The inflamed muscle slices and tumor tissue sections were incubated with rabbit anti-CD68 antibody (1:100, Abcam, USA) for 1 h, followed by Cy3-conjugated anti-rabbit secondary antibodies (1:200, Jackson Immuno Research Laboratories) for 30 min in the dark at room temperature. After washing with PBS, the slices were mounted with VECTASHIELD® mounting medium containing DAPI and coverslipped before visualization by epifluorescence microscopy (IX-81, Olympus).

2.6 Statistical analysis

The data are expressed as mean and standard deviation (SD). P-values < 0.05 were considered statistically significant.

3 Results and discussion

3.1 Biodistribution of ^{18}F-PBR06

The biodistribution data of ^{18}F-PBR06 in the inflammation and tumor models achieved at 120 min post-injection are presented in Fig. 2a. ^{18}F-PBR06 displayed higher uptake in the inflamed lesions (4.79 ± 0.48), whereas relatively lower uptake in the lung tumor tissues (1.55 ± 0.29) ($P < 0.001$) was found. Considering that accumulation in the brain, spleen, lung, blood, kidneys, right hind leg muscles, and intestines of the inflammation models was higher than of the lung cancer models (all $P < 0.05$), we used the target-to-nontarget ratios at 120 min post-injection in the animal models to explore the potential of ^{18}F-PBR06 to differentiate the inflamed lesions from lung tumor tissues.

The ratio of inflammation to blood (I/B) was 3.53 ± 0.26, and the ratio of tumor to blood (T/B) was 1.77 ± 0.35 ($P < 0.001$). The ratio of inflammation to muscle (I/M) was 2.33 ± 0.64, and the ratio of tumor to muscle (T/M) was 1.45 ± 0.14 ($P = 0.036$). The results revealed that ^{18}F-PBR06 had relatively high uptake in the inflammatory regions, and accumulation of ^{18}F-PBR06 in the lung tumor tissues was lower than in the inflammatory regions.

3.2 Micro-PET/CT imaging

The time activity curves obtained from the dynamic Micro-PET/CT imaging of ^{18}F-PBR06 are shown in Fig. 3, indicating that ^{18}F-PBR06 uptake in the inflamed muscles remained higher than normal muscles during the 90 min of dynamic Micro-PET/CT imaging (all $P < 0.05$). Moreover, ^{18}F-PBR06 uptake in the inflamed muscles remained higher than tumor tissues. Based on the biodistribution results, it further confirmed the specificity of ^{18}F-PBR06 for TSPO evaluation.

Figure 4 shows the Micro-PET/CT images of both tracers obtained from the inflammation and lung cancer models. All images were viewed from the top. ^{18}F-FDG showed high uptake in both inflamed muscles and lung tumor tissues. However, ^{18}F-PBR06 showed high uptake in inflamed muscles, but low uptake in lung tumor tissues. The results revealed that, compared to ^{18}F-FDG, ^{18}F-PBR06 showed superior specificity for inflammation.

3.3 Immunofluorescence

Immunofluorescence staining revealed macrophages in all specimens of the inflammation and lung cancer models. As shown in Fig. 5, macrophages in the inflammatory regions showed a higher fluorescence signal than the lung tumor tissue. These results revealed that the number of macrophages in the inflammatory regions was significantly higher than the lung tumor tissue. Therefore, the amount of TSPO in the inflammatory regions was also significantly higher than the lung tumor tissue. These results were consistent with the biodistribution and Micro-PET/CT imaging results.

3.4 Statistical analysis

The time activity curves obtained from the dynamic Micro-PET/CT imaging of ^{18}F-PBR06 revealed higher uptake in the inflamed muscles than lung tumor tissues during the 90-min imaging (all $P < 0.05$). Biodistribution demonstrated that the parameters of inflammation to blood in ^{18}F-PBR06 were significantly higher than those of tumor to blood ($P < 0.001$). Additionally, the parameters of inflammation to muscle in ^{18}F-PBR06 were higher than those of tumor to muscle ($P = 0.036$).

4 Discussion

^{18}F-FDG showed increased accumulation in the inflamed muscles and lung tumor tissues in this study, which was in agreement with previous reports, wherein ^{18}F-FDG has high sensitivity but low specificity [5].

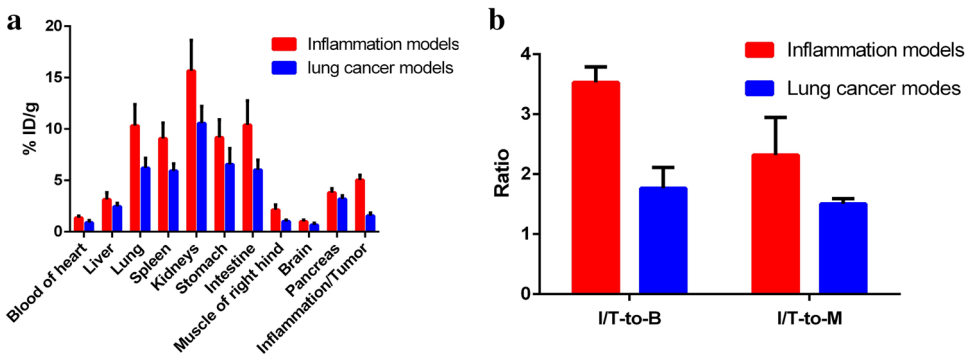

Fig. 2 **a** Biodistribution of ^{18}F-PBR06 at 2 h in inflammation and lung cancer models. **b** Parameters of target to nontarget at 2 h after injection in inflammation and lung cancer models (Color online)

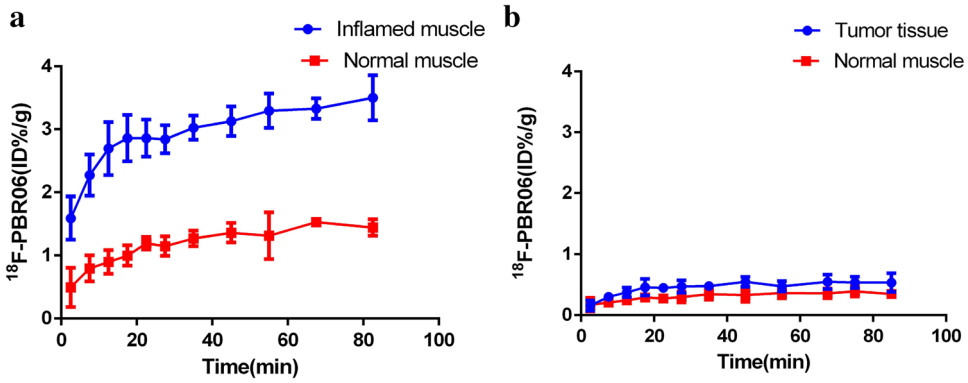

Fig. 3 **a** Time activity curves (TACs) of inflamed muscles during 90-min ^{18}F-PBR06 dynamic Micro-PET/CT imaging. **b** TACs of lung tumor tissues during 90-min ^{18}F-PBR06 dynamic Micro-PET/CT imaging (Color online)

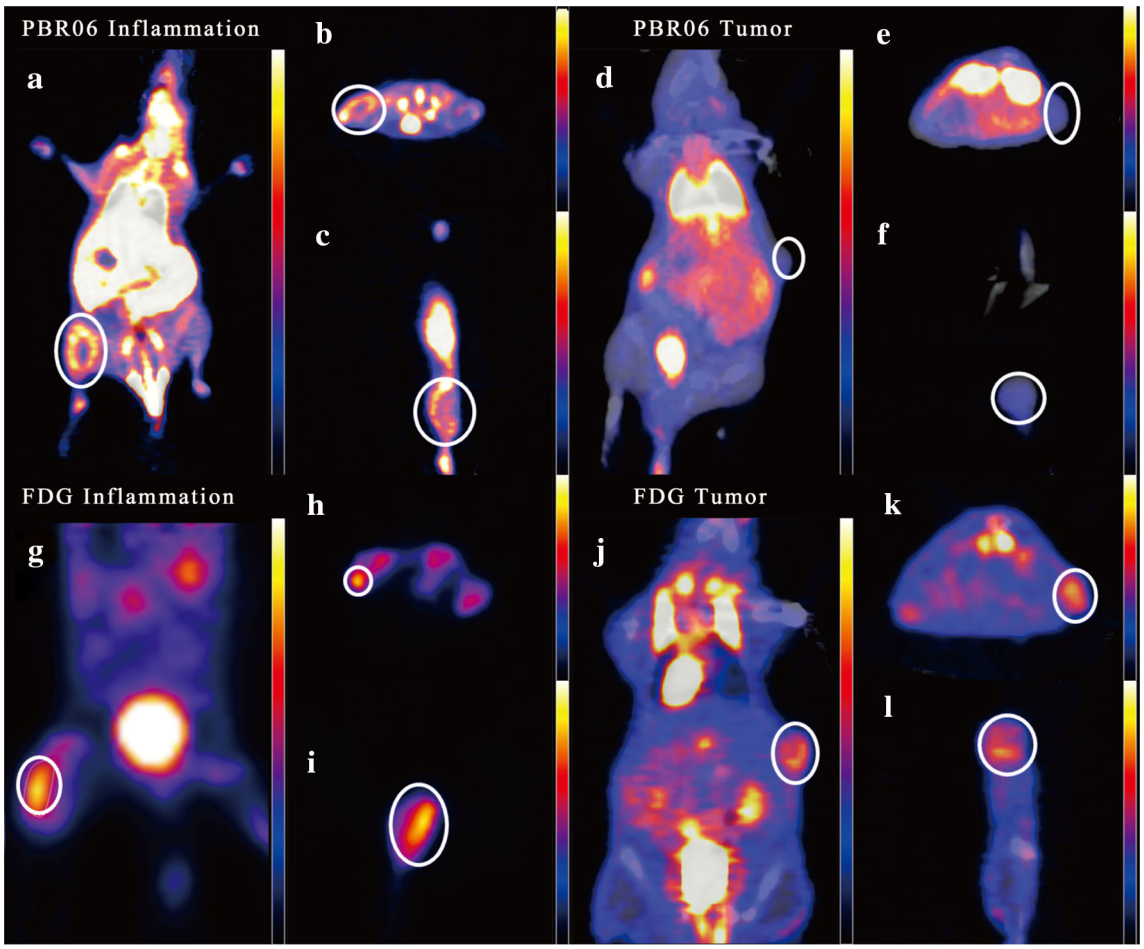

Fig. 4 ^{18}F-PBR06 and ^{18}F-FDG images of an inflammation model and lung cancer model. **a**, **d**, **g**, **j** Coronal views; **b**, **e**, **h**, **k** transverse views; and **c**, **f**, **i**, **l** sagittal views. ^{18}F-FDG accumulation showed high uptake during inflammation (**g**–**i**). ^{18}F-FDG accumulation showed high uptake in A549 tumor tissues (**j**–**l**). ^{18}F-PBR06 accumulation showed high uptake during inflammation (**a**–**c**). ^{18}F-PBR06 accumulation showed low uptake in A549 tumor tissues (**d**–**f**) (Color online)

However, ^{18}F-PBR06 exhibited high uptake during inflammation, but low uptake by the lung tumor tissues. Thus, ^{18}F-PBR06 can be considered as a higher specificity inflammation imaging tracer compared to ^{18}F-FDG. Furthermore, ^{18}F-PBR06 may have potential to differentiate between lung cancer and inflammation.

^{18}F-FDG has been used for diagnosis of inflammation and detection of infectious loci [18–20]. In the experimental inflammatory muscles, ^{18}F-FDG uptake was significantly higher than uptake in general muscle tissues. However, ^{18}F-FDG accumulated not only in the inflamed lesions, but also in a variety of tumors, including lung

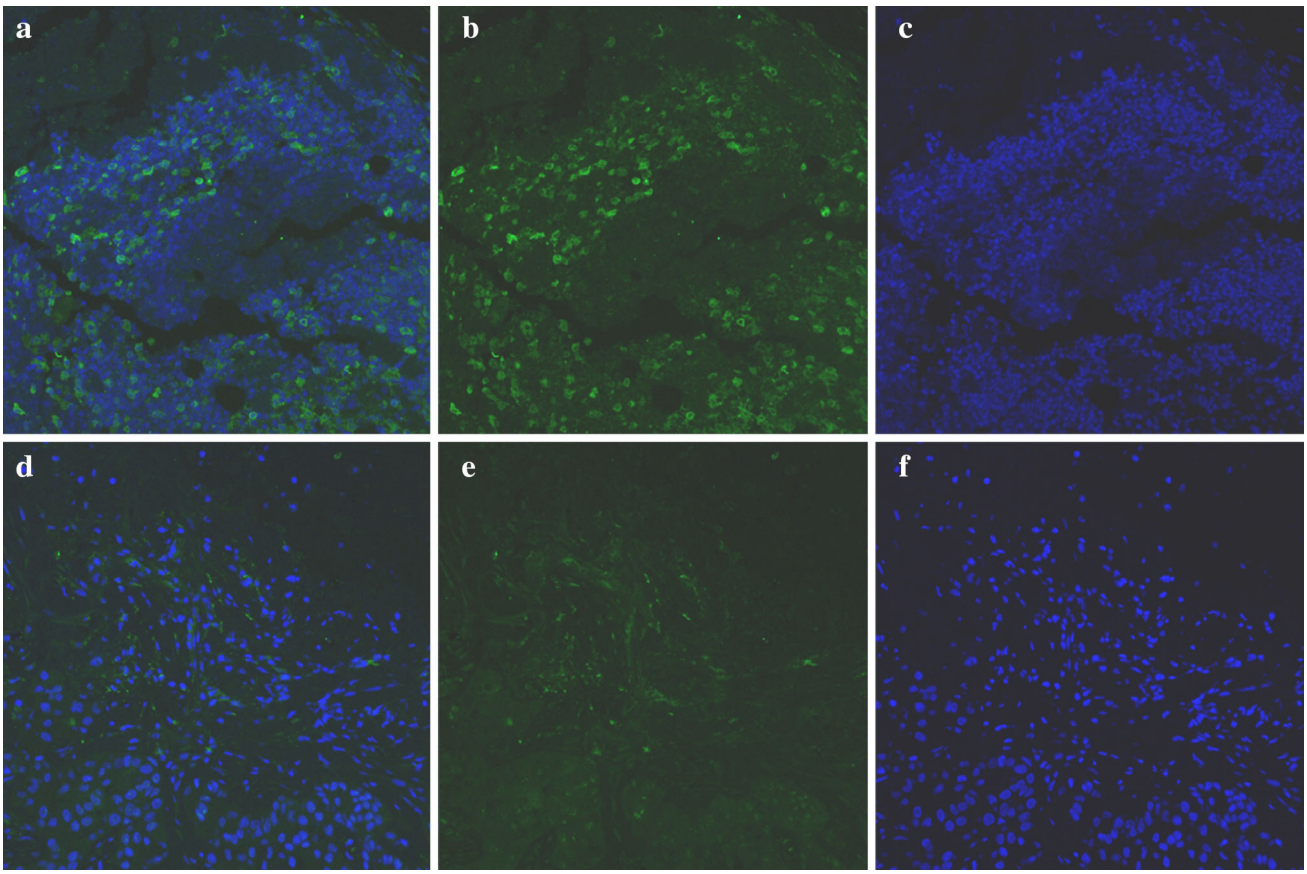

Fig. 5 Immunofluorescence of a specimen excised from an inflammation model and lung cancer model. A specimen from an inflamed muscle (**a**–**c**) and A549 tumor (**d**–**f**) (all samples were stained with $CD68^{+}$ and magnified × 200). The nuclei were stained blue, and TSPO was stained green. **a**, **d** Merged images, and the fluorescence signal of TSPO in inflamed muscle was much higher than the A549 tumor (Color online)

tumors [21, 22]. Furthermore, ^{18}F-FDG leads to high local uptake in inflammation and recurrent tumors for evaluation of changes in lesions after radio- or chemotherapy. Therefore, the inflammatory changes and recurrent tumors could not be differentiated from inflammation by ^{18}F-FDG PET/CT imaging [23, 24].

^{18}F-PBR06 is a novel radioligand that can characterize inflammation by measuring TSPO receptors; thus, ^{18}F-PBR06 PET/CT imaging can be a new tool for characterization of inflammation. Studies of some of the TSPO-specific tracers have been reported in neuroinflammatory diseases [25, 26] and inflammatory diseases of the peripheral tissues [27, 28]. In our study, we selected ^{18}F-PBR06 for its increased binding affinity, higher signal-to-noise ratio, and low lipophilicity, and it has been used in human studies.

In the current study, we used turpentine oil-induced inflammatory models to investigate the feasibility of ^{18}F-PBR06 PET/CT imaging in diagnosing inflammatory diseases. Thus, we selected day 7 after turpentine oil injection as the window for the macrophage infiltration in the inflammatory regions. In the acute inflammation phase, the cell population within the inflammatory regions primarily included lymphocytes and neutrophils, and the chronic inflammation phase mainly displayed monocytes and macrophages [29]. The turpentine oil would not be cleared easily, and hence, on days 3–6 post-turpentine oil injection, the inflammatory reaction would become chronic inflammation [30]. Therefore, ^{18}F-PBR06 uptake would reach a high level on day 7, and combined with the immunofluorescent images, we demonstrated that ^{18}F-PBR06 PET/CT imaging reflected macrophage infiltration during chronic inflammation. Therefore, the findings of the current study may indicate the feasibility of using ^{18}F-PBR06 PET/CT imaging for assessing inflammation via macrophage infiltration.

Compared to ^{18}F-FDG, ^{18}F-PBR06 exhibited lower uptake in lung tumor tissues, thereby designating ^{18}F-PBR06 as a specific tracer to characterize inflammation. In addition, ^{18}F-PBR06 showed low uptake in lung tumor tissues (1.55 ± 0.29), but high uptake during inflammation (4.79 ± 0.48). Previous reports showed elevated TSPO

levels within some specific tumors, such as ovary, breast, colon, and prostate cancer [31]. However, in this study, lung tumor tissues exhibited significantly low uptake of ^{18}F-PBR06 (T/B = 1.77 ± 0.35, T/M = 1.45 ± 0.14) as compared to the inflamed muscles (I/B = 3.53 ± 0.26, I/M = 2.33 ± 0.64). In ^{18}F-PBR06 Micro-PET/CT imaging, the lung tumor tissues showed lower uptake than the inflamed muscles (Fig. 4). Combined with the immunofluorescence results, the number of macrophages and the amount of TSPO in the inflammatory regions were significantly higher than the lung tumor tissues. There would also be macrophage infiltration in pulmonary inflammation nodules [32], suggesting that ^{18}F-PBR06 PET/CT imaging may allow for diagnosis of pulmonary inflammation nodules. Therefore, ^{18}F-PBR06 may be utilized to differentiate between peripheral lung cancer and inflammation nodules, thus enhancing accuracy in detection of pulmonary nodules.

Nevertheless, the present study had some limitations. For better comparisons of the data, this experiment could be improved by using mice bearing both inflammation and tumors in the same tissue. ^{18}F-PBR06 showed increased accumulation in the lung that was higher than uptake in the inflamed muscles; however, a previous study reported that ^{18}F-PBR06 showed very low uptake by the lung in the biodistribution of humans [12]. Moreover, a previous study reported that a TSPO-specific tracer might be a useful tool for evaluating lung inflammation [28]. Turpentine was used to induce inflammation in this study; however, turpentine inhalation might lead to pulmonary inflammation and empyema [33]. Therefore, pulmonary inflammation induced by turpentine inhalation might be the reason why ^{18}F-PBR06 showed increased accumulation in the lung in our study. Taken together, further verification is essential to evaluate the usefulness of ^{18}F-PBR06 in differentiating peripheral lung cancer and inflammation nodules.

5 Conclusion

In summary, ^{18}F-PBR06 exhibited a significant uptake in the inflamed muscles; however, uptake in the lung tumors was low as compared to ^{18}F-FDG. Therefore, this study confirmed that ^{18}F-PBR06 PET/CT imaging is useful in diagnosing inflammation, and ^{18}F-PBR06 can be considered as a superior inflammation imaging tracer of greater specificity compared to ^{18}F-FDG. Moreover, ^{18}F-PBR06 PET imaging may have potential in differentiating peripheral lung cancer and inflammation nodules based on its specificity, thereby enhancing the accuracy of pulmonary nodule detection.

References

1. C. Nathan, Points of control in inflammation. Nature **420**, 846–852 (2002). https://doi.org/10.1038/nature01320
2. C. Love, M.B. Tomas, G.G. Tronco et al., FDG PET of infection and inflammation. Radiographics **25**, 1357–1368 (2005). https://doi.org/10.1148/rg.255045122
3. M. Caglar, C. Yener, E. Karabulut, Value of CT, FDG PET-CT and serum tumor markers in staging recurrent colorectal cancer. Int. J. Comput. Assist. Radiol. Surg. **10**, 993–1002 (2015). https://doi.org/10.1007/s11548-014-1115-8
4. N. Seymour, G. Burkill, M. Harries, An analysis of true- and false-positive results of vocal fold uptake in positron emission tomography-computed tomography imaging. J. Laryngol. Otol. **132**, 270 (2018). https://doi.org/10.1017/S002221511700247X
5. I. Vlahos, K. Stefanidis, S. Sheard et al., Lung cancer screening: nodule identification and characterization. Transl. Lung Cancer Res. **7**, 288–303 (2018). https://doi.org/10.21037/tlcr.2018.05.02
6. C. Decotiis, Y. Hu, A.K. Greenberg et al., Inflammatory cytokines and non-small cell lung cancer in a CT-scan screening cohort: background review of the literature. Cancer Biomark. **16**, 219–233 (2016). https://doi.org/10.3233/CBM-150559
7. P. Yang, X.Y. Xu, X.J. Liu et al., The value of delayed (18)F FDG-PET imaging in diagnosis of solitary pulmonary nodules: a preliminary study on 28 patients. Quant. Imaging Med. Surg. **1**, 31–34 (2011). https://doi.org/10.3978/j.issn.2223-4292.2011.11.03
8. L.M. Coussens, Z. Werb, Inflammation and cancer. Nature **420**, 860–867 (2014). https://doi.org/10.1038/nature01322
9. C.J. Van Der Laken, E.H. Elzinga, M.A. Kropholler et al., Noninvasive imaging of macrophages in rheumatoid synovitis using 11C-(R)-PK11195 and positron emission tomography. Arthritis Rheumatol. **58**, 3350–3355 (2008). https://doi.org/10.1002/art.23955
10. Y.Y. Gent, A.E. Voskuyl, R.W. Kloet et al., Macrophage positron emission tomography imaging as a biomarker for preclinical rheumatoid arthritis: findings of a prospective pilot study. Arthritis Rheumatol. **64**, 62–66 (2012). https://doi.org/10.1002/art.30655
11. V. Papadopoulos, M. Baraldi, T.R. Guilarte et al., Translocator protein (18 kDa): new nomenclature for the peripheral-type benzodiazepine receptor based on its structure and molecular function. Trends Pharmacol. Sci. **27**, 402–409 (2006). https://doi.org/10.1016/j.tips.2006.06.005
12. Y. Fujimura, Y. Kimura, F.G. Simeon et al., Biodistribution and radiation dosimetry in humans of a new PET ligand, (18)F-PBR06, to image translocator protein (18 kDa). J. Nucl. Med. **51**, 145–149 (2010). https://doi.org/10.2967/jnumed.109.068064
13. S. Zhang, L. Yang, X. Ling et al., Tumor mitochondria-targeted photodynamic therapy with a translocator protein (TSPO)-specific photosensitizer. Acta Biomater. **28**, 160–170 (2015). https://doi.org/10.1016/j.actbio.2015.09.033
14. M. Imaizumi, E. Briard, S.S. Zoghbi et al., Kinetic evaluation in nonhuman primates of two new pet ligands for peripheral benzodiazepine receptors in brain. Synapse **61**, 595–605 (2010). https://doi.org/10.1002/syn.20394
15. F.M. Lartey, G.O. Ahn, B. Shen et al., PET imaging of stroke-induced neuroinflammation in mice using [18F]PBR06. Mol. Imaging Biol. **16**, 109–117 (2014). https://doi.org/10.1007/s11307-013-0664-5
16. E. Briard, S.S. Zoghbi, F.G. Simeon et al., Single-step high-yield radiosynthesis and evaluation of a sensitive 18F-labeled ligand for imaging brain peripheral benzodiazepine receptors with PET. J. Med. Chem. **52**, 688–699 (2009). https://doi.org/10.1021/jm8011855

17. M. Wang, M. Gao, K.D. Miller et al., Synthesis of [^{11}C]PBR06 and [18F]PBR06 as agents for positron emission tomographic (PET) imaging of the translocator protein (TSPO). Steroids **76**, 1331–1340 (2011). https://doi.org/10.1016/j.steroids.2011.06.012
18. S. Vaidyanathan, C.N. Patel, A.F. Scarsbrook et al., FDG PET/CT in infection and inflammation—current and emerging clinical applications. Clin. Radiol. **70**, 787–800 (2015). https://doi.org/10.1016/j.crad.2015.03.010
19. A.M. Chacko, S. Watanabe, K.J. Herr et al., 18F-FDG as an inflammation biomarker for imaging dengue virus infection and treatment response. JCI Insight (2017). https://doi.org/10.1172/jci.insight.93474
20. M. Meyer, P. Fernandez, P. Zanotti-Fregonara, 18F-FDG imaging of chronic inflammation associated with promontofixation of the uterus. Clin. Nucl. Med. **42**, 42–43 (2017). https://doi.org/10.1097/RLU.0000000000001420
21. S. Han, S. Woo, H.S. Chong et al., A systematic review of the prognostic value of texture analysis in 18F-FDG PET in lung cancer. Ann. Nucl. Med. (2018). https://doi.org/10.1007/s12149-018-1281-9
22. J. Toyohara, P.H. Elsinga, K. Ishiwata et al., Evaluation of 4′-[methyl-11C] thiothymidine in a rodent tumor and inflammation model. J. Nucl. Med. **53**, 488–494 (2012). https://doi.org/10.2967/jnumed.111.098426
23. S. Wagner, H.J. Breyholz, C. Holtke et al., A new 18F-labelled derivative of the MMP inhibitor CGS 27023A for PET: radiosynthesis and initial small-animal PET studies. Appl. Radiat. Isot. **67**, 606–610 (2009). https://doi.org/10.1016/j.apradiso.2008.12.009
24. O. Devinsky, A. Vezzani, S. Najjar et al., Glia and epilepsy: excitability and inflammation. Trends Neurosci. **36**, 174–184 (2013). https://doi.org/10.1016/j.tins.2012.11.008
25. H. Boutin, C. Prenant, R. Maroy et al., [18F]DPA-714: direct comparison with [11C]PK11195 in a model of cerebral ischemia in rats. PLoS ONE **8**, e56441 (2013). https://doi.org/10.1371/journal.pone.0056441
26. D. Harhausen, V. Sudmann, U. Khojasteh et al., Specific imaging of inflammation with the 18 kDa translocator protein ligand DPA-714 in animal models of epilepsy and stroke. PLoS ONE **8**, e69529 (2013). https://doi.org/10.1371/journal.pone.0069529
27. O. Gaemperli, J. Shalhoub, D.R. Owen et al., Imaging intraplaque inflammation in carotid atherosclerosis with 11C-PK11195 positron emission tomography/computed tomography. Eur. Heart J. **33**, 1902–1910 (2012). https://doi.org/10.1093/eurheartj/ehr367
28. A. Hatori, J. Yui, T. Yamasaki et al., PET imaging of lung inflammation with [18F]FEDAC, a radioligand for translocator protein (18 kDa). PLoS ONE **7**, e45065 (2012). https://doi.org/10.1371/journal.pone.0045065
29. M.A. Ingersoll, A.M. Platt, S. Potteaux et al., Monocyte trafficking in acute and chronic inflammation. Trends Immunol. **32**, 470–477 (2011). https://doi.org/10.1016/j.it.2011.05.001
30. J. Toyohara, M. Sakata, K. Oda, Longitudinal observation of [11C]4DST uptake in turpentine-induced inflammatory tissue. Nucl. Med. Biol. **40**, 240–244 (2013). https://doi.org/10.1016/j.nucmedbio.2012.10.008
31. C. Wu, X. Yue, L. Lang et al., Longitudinal PET imaging of muscular inflammation using 18F-DPA-714 and 18F-Alfatide II and differentiation with tumors. Theranostics **4**, 546–555 (2014). https://doi.org/10.7150/thno.8159
32. C.H. Xu, J.S. Xue, X.W. Zhang et al., The value of macrophage inhibitory cytokine-1 level in differentiating benign from malignant solitary pulmonary nodules. Clin. Respir. J. **12**, 1473–1478 (2018). https://doi.org/10.1111/crj.12693
33. A.J. Khan, R.P. Akhtar, Z.S. Faruqui, Turpentine oil inhalation leading to lung necrosis and empyema in a toddler. Pediatr. Emerg. Care **22**, 355–357 (2006). https://doi.org/10.1097/01.pec.0000215371.48859.fd